The Iranian Journal of Mechanical Engineering Transactions of ISME
Journal homepage: https://jmee.isme.ir/
Vol. 26, No. 2, 2025, pp. 35-56

Research Paper

DOI: https://doi.org/10.30506/jmee.2024.2041811.1362

Computation of SIF for Several Moving Cracks in an Orthotropic Layer Bonded to a Functionally Graded Piezoelectric Coating

Mohammad Hassani*
PhD Student

Mojtaba Mahmoudi Monfared†
Associate Professor

In this paper, the dynamic stress intensity factors (DSIFs) in an orthotropic strip coated by a functionally graded piezoelectric (FGP) containi8ng several moving cracks has been studied. The distributed dislocation method (DDM) is extended to construct integral equations for the several cracks. At first, the stress fields in an orthotropic strip coated by FGP containing a single dislocation are calculated. Then, by use of distributed dislocation density on the faces of cracks, systems of singular integral equations with Cauchy type singularity are obtained. Finally, the integral equations are solved with an appropriate numerical method to specify the dislocation density and then DSIFs at the crack tips. The primary objective of this paper is to investigate the effects types of loading, the position of cracks relative to each other, crack speed and nonhomogeneity parameter on the DSIFs.

Keywords: Orthotropic substrate, FGP coating, Distributed dislocation technique, Dynamic stress intensity factors, Several moving cracks

1 Introduction

The first explanation of smart structures has been generally discussed roughly four decades ago. The so-called smart structures are correlated to the developments in advanced structures which are widely used in automobiles, shipbuilding industries, aeronautical and space sciences. Moreover, smart structures made by materials such as piezoelectric and piezo-magnetic, have various applications in vibration control, shape morphing, active optics and structural health monitoring [1].

* PhD Student, Department of Mechanical Engineering, Do.C., Islamic Azad University, Dorud, Iran, m.hasani@khoiau.ac.ir

† Corresponding Author, Associate Professor, Department of Mechanical Engineering, Has.C., Islamic Azad University, Hashtgerd, Iran, mo_m_monfared@iau.ac.ir

Received: 2024/09/23, Revised: 2024/11/26, Accepted: 2024/12/09

On the other side, functionally graded materials (FGMs) have considerably improved, for example, the thermal shock resistance, corrosion resistance, and fatigue life of the structures [2, 3].

Hence, by applying the concept of FGMs to the smart materials it is feasible to enhance the reliability of piezoelectric structures which are known as functionally graded piezoelectric materials (FGPMs) [4]. Layered materials are widely used in various products to improve structural efficiency, such as strength and stability. In many applications, the orthotropic substrate with gradient piezoelectric layers is used to improve the mechanical behavior. However, such structures may contain several flaws and defects, especially in the form of propagating cracks which may cause to a catastrophic failure. Eventually, thorough comprehension of fracture behavior for the aforementioned structures is indispensable. Ma et al. [5] studied the moving mode III interface crack problem in bonded dissimilar piezoelectric materials. The effects of electric loading on the stress intensity factors (SIFs) were examined. Shin and Lee [6] analyzed a moving interface crack between two dissimilar FGP layers. The effect of electromechanical loading on the SIFs were obtained and shown to have significant impact on the SIFs. Lapusta et al. [7] investigated a permeable moving crack at the interface of a piezoelectric bi-material. The stress and electric intensity factors at the crack tips were found and the influence of the electric traction on the crack faces was investigated. As an example of an embedded crack, Monfared and Ayatollahi, Hejazi et al. [8-10] studied the dynamic stress intensity factors of multiple cracks in the FG orthotropic half-plane under time-harmonic loading, and an orthotropic half-plane in addition to an orthotropic strip bonded to an FG layer under anti-plane loading. In these investigations the material properties were assumed to vary exponentially along the vertical axis. The effects of material properties and crack configuration on the SIFs were studied. Nguyen et al. [11] studied the transient dynamic stress intensity factors for the two-dimensional problem of isotropic solids and orthotropic composites by the extended mesh-free method. Rokne et al. [12] investigated the dynamic behavior of a moving mode III Griffith crack in a piezoelectric layer sandwiched between two elastic infinite spaces. The SIFs at the crack tips and energy release rate were obtained numerically. Podgórski [13] investigated the fracture ana ysis of brittle composite materials assuming the plane stress state. The mediums were modelled as an isotropic matrix with the help of finite element method. Bagheri et al. [14] presented an analytical solution for moving cracks in an FGP strip. The effects of the crack speed and material properties on the SIFs were studied. Lee et al. [15] worked on anti-plane interfacial Yoffe-crack between a piezoelectric and two orthotropic layers. Their investigation showed that the dynamic stress intensity factors depend on crack length, ratios of stiffness, layers thickness and direction of electrical loads.

Monfared [16] studied the stress intensity factors for multiple interface cracks under mode III deformation. The crack geometry and material properties on the SIFs were studied. Interaction between of multiple interface cracks in an FGM orthotropic layer and orthotropic substrate under concentrated loads analyzed by Hassani and Monfared [17]. Haghiri et al. [18] presented a set of dynamic analysis for multiple parallel and perpendicular cracks in a FG orthotropic half-plane under anti-plane loading. The effects of FG parameter and shear modulus ratio on the dynamic overshoot of SIFs were studied. Shin et al. [19] solved the anti-plane moving crack in an FGP layer between two dissimilar piezoelectric strips. The computed results showed that certain direction, magnitude of the electric loading and accrue of the thickness of the FGP interface layer correlate to the resistance of crack propagation in the FGP interface layer. Hu and Chen [20] investigated the mode III problem of the interface moving crack between magneto-electro-elastic and FG elastic layers under anti-plane loading and in-plane magnetic and electric loading. Jin and Zhong [21] examined the propagation of a moving mode III crack in a FGP strip. It is assumed that the crack surfaces are permeable. It is found that the velocity of the crack has a great impact on the dynamic SIFs.

The stress field around various blunt notches by means of the digital image correlation experimentally studied in [22, 23] under mixed mode loading. The effects of higher order terms on the stress distribution at the vicinity of the sharp corner of two bonded dissimilar materials under anti-plane shear loading investigated by Bahrami et al. [24]. An analytical stress solution for the bi-material V-notches with end hole studied by Alavi et al. [25].
In this paper we used the DDM which is a powerful semi-analytical method for calculating accurate solutions to plane crack problems based on the principle of superposition. In fact, the technique is excellent for solutions of complex crack patterns [9] and makes it an ideal tool for exploring problems involving inclusions, interfaces, pores, and similar features [16].
Due to the reviewed literatures which are mentioned above, it is found that there is not a promising investigation of the multiple moving cracks in an orthotropic strip bonded to an FGP layer and, thereby, this analysis for fracture mechanics is necessary. This paper aims to fulfill the mentioned gap. Hence, by utilizing the Fourier transformation, the Cauchy type singular integral equations based on the distributed dislocation density on the crack surfaces will be appeared. Then, these equations are solved numerically and the stress intensity factors will be obtained at the crack tips.

2 Fundamental formulations

An orthotropic substrate with thickness h_2 bonded to a FGP layer poled in the z direction with thickness h_1 as shown in Figure (1). According to the Figure (1), a Volterra-type screw dislocation moves along the $X-$axis with the constant velocity V. The displacement field and the electric field components are

$$\begin{aligned} &u = 0, v = 0, w = w\,(X,Y) \\ &E_x = E_x(X,Y), E_y = E_y(X,Y),\ E_z = 0 \end{aligned} \tag{1}$$

and the electric fields have a relation with the electrical potential $\phi(x,y)$ as follows

$$E_x = -\frac{\partial \phi}{\partial X}, E_y = -\frac{\partial \phi}{\partial Y} \tag{2}$$

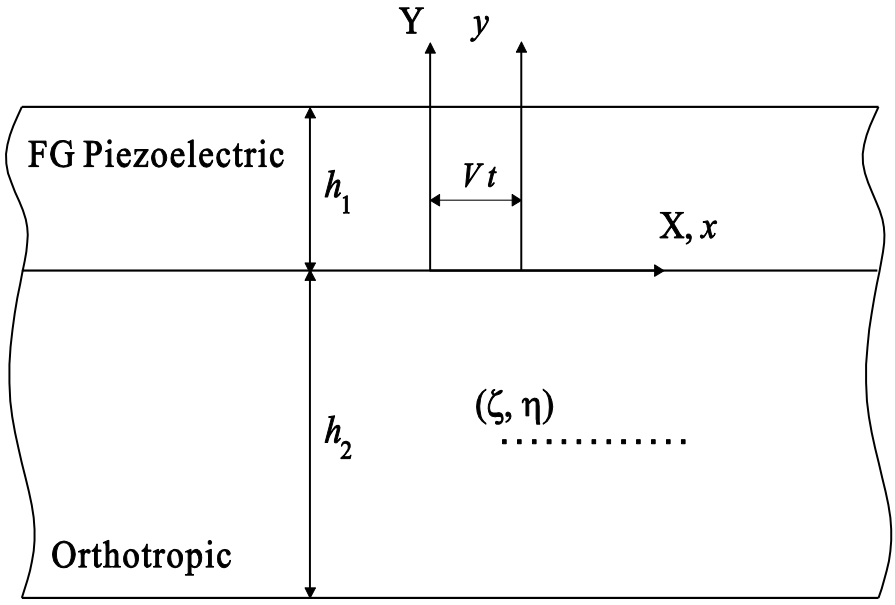

Figure 1 Schematic view of a cracked orthotropic layer with FG piezoelectric coating

The constitutive equations for the in-plane electric fields coupling with the anti-plane elastic fields of the FGP layer in the region $0 < y < h_1$ are given by

$$\begin{aligned}
\sigma_{zx1}(X,Y) &= c_{44}(Y)\frac{\partial w_1(X,Y)}{\partial X} + e_{15}(Y)\frac{\partial \phi_1(X,Y)}{\partial X},\\
\sigma_{zy1}(X,Y) &= c_{44}(Y)\frac{\partial w_1(X,Y)}{\partial Y} + e_{15}(Y)\frac{\partial \phi_1(X,Y)}{\partial Y},\\
D_{x1}(X,Y) &= e_{15}(Y)\frac{\partial w_1(X,Y)}{\partial x} - d_{11}(Y)\frac{\partial \phi_1(X,Y)}{\partial X},\\
D_{y1}(X,Y) &= e_{15}(Y)\frac{\partial w_1(X,Y)}{\partial Y} - d_{11}(Y)\frac{\partial \phi_1(X,Y)}{\partial Y}.
\end{aligned} \tag{3}$$

in which ϕ_1 are the components of electric potential in region $0 < y < h_1$, $D_{x1}(X,Y)$ and $D_{y1}(X,Y)$ are the components of electric displacements. Moreover, $c_{44}(Y)$, $d_{11}(Y)$ and $e_{15}(Y)$ are the shear modulus, dielectric and the piezoelectric constants, respectively.
The equilibrium equation for the stress components and the Maxwell equation for the electric displacement components are

$$\begin{aligned}
&\frac{\partial \sigma_{xz1}(X,Y)}{\partial X} + \frac{\partial \sigma_{yz1}(X,Y)}{\partial Y} = \rho_{piezo}\frac{\partial^2 w_1(X,Y)}{\partial t^2},\\
&\frac{\partial D_{x1}(X,Y)}{\partial X} + \frac{\partial D_{y1}(X,Y)}{\partial Y} = 0
\end{aligned} \tag{4}$$

where ρ_{piezo} is the mass density of piezoelectric layer. By substituting Eq. (3) into Eq. (4) we have

$$\begin{aligned}
&c_{44}(Y)\Delta w_1 + e_{15}(Y)\Delta\phi_1 + \frac{\partial c_{44}(Y)}{\partial Y}\frac{\partial w_1}{\partial Y} + \frac{\partial e_{15}(Y)}{\partial Y}\frac{\partial \phi_1}{\partial Y} = \rho_{piezo}\frac{\partial^2 w_1}{\partial t^2},\\
&e_{15}(Y)\Delta w_1 - d_{11}(Y)\Delta\phi_1 + \frac{\partial e_{15}(Y)}{\partial Y}\frac{\partial w_1}{\partial Y} - \frac{\partial d_{11}(Y)}{\partial Y}\frac{\partial \phi_1}{\partial Y} = 0,\\
&\left(\Delta = \frac{\partial^2}{\partial X^2} + \frac{\partial^2}{\partial Y^2}\right)
\end{aligned} \tag{5}$$

The properties of FG piezoelectric are assumed to be vary in the $y-$ direction and described in terms of exponential functions along the thickness of layer as follow

$$[c_{44}(Y), e_{15}(Y), d_{11}(Y), \rho_{piezo}(Y)] = [c_{44}^0, e_{15}^0, d_{11}^0, \rho_{piezo}^0]\exp(2\kappa Y) \tag{6}$$

where $c_{44}^0, e_{15}^0, d_{11}^0$ and ρ_{piezo}^0 are material constants at $y = 0$. Also, $\kappa$is the nonhomogeneity parameter. By replacing Eq. (6) into the Eq. (5) we obtain

$$\begin{aligned}
&c_{44}^0\Delta w_1 + e_{15}^0\Delta\phi_1 + 2\kappa c_{44}^0\frac{\partial w_1}{\partial Y} + 2\kappa e_{15}^0\frac{\partial \phi_1}{\partial Y} = \rho_{piezo}^0\frac{\partial^2 w_1}{\partial t^2},\\
&e_{15}^0\Delta w_1 - d_{11}^0\Delta\phi_1 + 2\kappa e_{15}^0\frac{\partial w}{\partial Y} - 2\kappa d_{11}^0\frac{\partial \phi_1}{\partial Y} = 0
\end{aligned} \tag{7}$$

For analyzing the moving crack with the constant velocity *V*, we consider the problem in a steady state form with a Galilean transformation as follows

$$X = x + Vt,\ Y = y,\ \frac{\partial}{\partial t} = V\frac{\partial}{\partial x} \tag{8}$$

in which (x, y, t) is the moving coordinate system related to the moving dislocation. With the help of the Eq. (8), the Eq. (7) can be written within the new coordinate system(x, y) as follows:

$$\begin{aligned} &c_{44}^0\,\Delta w_1 + e_{15}^0\,\Delta\phi_1 + 2\,\kappa\,c_{44}^0\,\frac{\partial w_1}{\partial y} + 2\,\kappa\,e_{15}^0\,\frac{\partial \phi_1}{\partial y} = V^2\rho_{piezo}^0\,\frac{\partial^2 w_1}{\partial x^2}, \\ &e_{15}^0\,\Delta w_1 - d_{11}^0\,\Delta\phi_1 + 2\,\kappa\,e_{15}^0\,\frac{\partial w_1}{\partial y} - 2\,\kappa\,d_{11}^0\,\frac{\partial \phi_1}{\partial y} = 0 \end{aligned} \tag{9}$$

Utilizing the Bleustein function [26]

$$\psi_1(x, y) = \phi_1 - \alpha w_1, \alpha = e_{15}^0/d_{11}^0 \tag{10}$$

The Eq. (9) are decoupled to the following form

$$\mu^2\,\frac{\partial^2 w_1}{\partial x^2} + \frac{\partial^2 w_1}{\partial y^2} + 2\kappa\,\frac{\partial w_1}{\partial y} = 0, \Delta\psi_1 + 2\kappa\,\frac{\partial \psi_1}{\partial y} = 0 \tag{11}$$

in which

$$\mu^2 = (1 - \beta V^2), \kappa = \frac{\rho_{piezo}}{c_{44} + \alpha e_{15}} \tag{12}$$

Therefore, by virtue of new variables (ψ_1, w_1) the constitutive Eq. (3) can be written as follows

$$\begin{aligned} &\sigma_{zx1} = [c_{44}(y) + \alpha e_{15}(y)]\,\frac{\partial w_1}{\partial x} + e_{15}(y)\,\frac{\partial \psi_1}{\partial x}, \quad D_{x1} = -d_{11}(y)\,\frac{\partial \psi_1}{\partial x}, \\ &\sigma_{zy1} = [c_{44}(y) + \alpha e_{15}(y)]\,\frac{\partial w_1}{\partial y} + e_{15}(y)\,\frac{\partial \psi_1}{\partial y}, \; D_{y1} = -d_{11}(y)\,\frac{\partial \psi_1}{\partial y}. \end{aligned} \tag{13}$$

2.1 Formulations for orthotropic layer

The constitutive equations on anti-plane deformation for orthotropic layer $(-h_2 < y < 0)$ are given by

$$\begin{aligned} &\sigma_{zxi}(X, Y, t) = G_x\,\frac{\partial w_i(X,Y,t)}{\partial X}, \\ &\sigma_{zyi}(X, Y, t) = G_y\,\frac{\partial w_i(X,Y,t)}{\partial Y}, i = 2,3 \end{aligned} \tag{14}$$

in which G_x and G_y are material constants of orthotropic layer in the $x-$ and $y-$ directions, respectively. Substituting the stress components in the equation of motion yields

$$G_x\,\frac{\partial^2 w_i(X,Y,t)}{\partial X^2} + G_y\,\frac{\partial^2 w_i(X,Y,t)}{\partial Y^2} = \rho_{Ortho}\,\frac{\partial^2 w_i(X,Y,t)}{\partial\, t^2}, i = 2,3 \tag{15}$$

By utilizing Galilean transformation (8) we have

$$\gamma^2\,\frac{\partial^2 w_i(x,y)}{\partial x^2} + \frac{\partial^2 w_i(x,y)}{\partial y^2} = 0, i = 2,3 \tag{16}$$

in which,$\gamma^2 = g^2 - \frac{V^2}{C_p^2}$, $C_p^2 = \frac{G_y}{\rho_{Ortho}}$.and $g^2 = \frac{G_x}{G_y}$. The following conditions must be satisfied when no traction is applied on the boundaries ($y = h_1$) and ($y = -h_2$) of the layers.

$$\sigma_{zy1}(x, h_1) = 0, \sigma_{zy3}(x, -h_2) = 0 \tag{17}$$

Furthermore, the continuity and limiting conditions for the screw dislocation may be expressed as

$$\begin{aligned} &\sigma_{zy2}(x, \eta^+) = \sigma_{zy3}(x, \eta^-), \ \ \sigma_{zy1}(x, 0^+) = \sigma_{zy2}(x, 0^-), \\ &D_y(x, 0) = 0, \ D_y(x, h_1) = 0, \ \ \ w_1(x, 0^+) = w_2(x, 0^-), \\ &w_2(x, \eta^+) - w_3(x, \eta^-) = b_z H(x - \zeta) \end{aligned} \tag{18}$$

in which $H(.)$ is the Heaviside step-function and b_z is the Burgers vector. The Eqs. (11) and (16) may be solved by means of the complex Fourier transform which is defined as

$$f^*(s) = \int_{-\infty}^{+\infty} f(x)\ e^{isx} dx, \ f(x) = \frac{1}{2\pi} \int_{-\infty}^{+\infty} f^*(s)\ e^{-isx} ds \tag{19}$$

First the displacement components can be obtained from conditions (17) and (18), and then the stress fields in the orthotropic layer with the help of Eq. (14) will be calculated. The stress components are singular at the vicinity of the dislocation. The asymptotic behavior of the stresses can be obtained as $s \to \infty$. After separating the singular terms, the stress components in region $\eta < y < 0$ may be expressed as follows

$$\begin{aligned} \sigma_{zx2}(x, y) = \frac{b_z G_x}{\pi} \{ &\frac{\gamma(y-\eta)}{2[(x-\zeta)^2 + \gamma^2(y-\eta)^2]} \\ &- \int_0^\infty \left(\frac{Q_{11}}{E} [Q_{12} + Q_{13}] + \frac{e^{s\gamma(\eta - y)}}{2} \right) \cos[s(x-\xi)] ds\}, \\ \sigma_{zy3}(x, y) = -\frac{b_z G_y \gamma}{\pi} \{ &\frac{(x-\zeta)}{2[(x-\zeta)^2 + \gamma^2(y-\eta)^2]} \\ &+ \int_0^\infty \left(\frac{Q_{41}}{E} [Q_{42} - Q_{43}] - \frac{e^{s\gamma(y-\eta)}}{2} \right) \sin[s(x-\xi)] ds\} \end{aligned} \tag{20a}$$

and in region $\eta < y < -h_2$ the stress components are

$$\begin{aligned} \sigma_{zx3}(x, y) = \frac{b_z G_x}{\pi} \{ &\frac{\gamma(\eta-y)}{2[(x-\zeta)^2 + \gamma^2(y-\eta)^2]} \\ &+ \int_0^\infty \left(\frac{Q_{31}}{E} [Q_{32} - Q_{33}] - \frac{e^{s\gamma(y-\eta)}}{2} \right) \cos[s(x-\xi)] ds\}, \\ \sigma_{zy3}(x, y) = -\frac{b_z G_y \gamma}{\pi} \{ &\frac{(x-\zeta)}{2[(x-\zeta)^2 + \gamma^2(y-\eta)^2]} \\ &+ \int_0^\infty \left(\frac{Q_{41}}{E} [Q_{42} - Q_{43}] - \frac{e^{s\gamma(y-\eta)}}{2} \right) \sin[s(x-\xi)] ds\} \end{aligned} \tag{20b}$$

where the functions Q_{ij}, χ and α_1 are given in the "**Appendix A**" and the parameter E is

$$\begin{aligned} \mathrm{E} = \mathrm{G_y}\gamma\chi\cosh(\mathrm{h_1}\chi)\sinh(\mathrm{sh_2}\gamma) \ + [\mathrm{s}\alpha_1\mu^2\cosh(\mathrm{sh_2}\gamma) \\ - \mathrm{G_y}\kappa\gamma\sinh(\mathrm{sh_2}\gamma)]\sinh(\mathrm{h_1}\chi) \end{aligned} \tag{21}$$

3 Different tractions on the boundary edges

In this section, three different loadings are discussed. First, a solution to the moving point loads is given in subsection (3.1). Then, two various uniforms shear tractions defined by pure mechanical loading and dielectric displacement on the boundary edges are illustrated in subsection (3.2).

3.1 Electromechanical point loads

The orthotropic layer and the FGP coating are under an anti-plane pure mechanical and in-plane electrical point loads with the magnitude τ_0 and D_0 respectively. The boundary condition may be written as

$$\begin{aligned}&\sigma_{zy3}(x,-h_2)=\tau_0\delta(x), D_y(x,h_1)=D_0\delta(x),\\&\sigma_{zy1}(x,h_1)=\tau_0\delta(x), D_y(x,0^+)=D_0\delta(x).\end{aligned} \tag{22}$$

where $\delta(.)$ is the Dirac delta function. With the help of Fourier transform Eq. (19), and boundary conditions (22), a procedure similar to the dislocation solution, the stress components may be found as

$$\begin{aligned}\sigma_{zx2}(x,y)=&-\frac{G_x D_0 e_{15}}{d_{11}\pi(\mu\alpha_1+\gamma G_y)}\left(\frac{x}{x^2+(y\gamma)^2}\right)\\&-\int_0^\infty\{\frac{e^{-\kappa h_1}g^2}{2s\gamma F}[L_{11}-L_{12}-L_{13}+L_{14}+L_{15}-L_{16}]\\&+\frac{G_x D_0 e_{15}}{d_{11}\pi(\mu\alpha_1+\gamma G_y)}e^{s\gamma y}\}\sin(sx)ds\},\\\sigma_{zy2}(x,y)=&\frac{\gamma G_y D_0 e_{15}}{d_{11}\pi(\mu\alpha_1+\gamma G_y)}\left(\frac{y\gamma}{x^2+(y\gamma)^2}\right)\\&+\int_0^\infty\{\frac{e^{-\kappa h_1}}{F}[L_{21}-L_{22}+L_{23}+L_{24}]+\frac{\gamma G_y D_0 e_{15}}{d_{11}\pi(\mu\alpha_1+\gamma G_y)}e^{s\gamma y}\}\cos(sx)ds\}.\end{aligned} \tag{23}$$

where the functions F and L_{ij} are given in the "**Appendix B**" and parameters χ and α_1 are the same parameters defined in Eq. (20).

3.2 Uniform shear tractions

Two different kind of uniform tractions are applied to the boundaries. Case I, illustrates the constant shear traction on the boundaries defined by pure mechanical loading τ_0 and dielectric displacement D_0 Lee et al. [15]. Case II, depicts the stresses for the uniform traction defined by pure mechanical loading τ_0 without the effect of dielectric displacement on the crack faces which is considered in many investigations mentioned in the literature. The boundary condition may be written as

$$\begin{aligned}&\sigma_{zy3}(x,-h_2)=\tau_{eq}, D_y(x,h_1)=D_0,\\&\sigma_{zy1}(x,h_1)=\tau_{eq}, D_y(x,0^+)=D_0.\\&\tau_{eq}=\begin{cases}\frac{\alpha_1}{c_{44}}\tau_0-\frac{e_{15}}{d_{11}}D_0(\text{Case I})\\\tau_0(\text{Case II})\end{cases}\end{aligned} \tag{24}$$

4 Multiple moving crack formulations

The solution for the dislocation can be employed to analyze layers containing multiple moving cracks. Thereby, the moving cracks configurations with coordinates (x_i, y_i) may be described in parametric form as fallow

$$x_i = x_{0i} + a_i\omega, y_i = y_{0i}, -1 \le \omega \le 1, i = 1,2,\dots,N. \tag{25}$$

where a_i and (x_{0i}, y_{0i}) are the half-length and the center of the cracks respectively. The stress components on the local coordinates are as follows

$$\sigma_{yz}(x_i(\omega), y_i) = \sigma_{yz}, \;\; i = 1,2,\dots,N. \tag{26}$$

At this step, suppose a dislocation with unknown dislocation density $B_{zj}(p)$ is distributed on the infinitesimal segment da_j located on the surface of the j-th crack. The anti-plane traction components on the i-th crack surface due to the presence of the distributed dislocations on the face of all N moving cracks yield

$$\sigma_{yz}(x_i(\omega), y_i) = \sum_{j=1}^{N} \int_{-1}^{+1} k_{ij}(\omega, p)\, a_j B_{zj}(p) dp\,, \;\; i = 1,2,\dots,N. \tag{27}$$

With respect to Buckner's principle Hills et al. [27], the left side of Eq. (27), after changing the sign, is the traction caused by external loading on the uncracked medium at the presumed surfaces of cracks (see section 3). Besides, the kernels $k_{ij}(\omega, p)$appeared in Eq. (27) are the coefficients of b_z in Eq. (20) for each region. The crack opening displacement across the j-th crack can be written using the definition of dislocation as

$$w_j^-(\omega) - w_j^+(\omega) = \int_{-1}^{\omega} a_j B_{zj}(p) dp\,, j = 1,2,\dots,N. \tag{28}$$

The displacement fields must be a single-valued, as a consequence, the following closure conditions for embedded cracks should be employed

$$\int_{-1}^{1} B_{zj}(p)\, dp = 0, j = 1,2,\dots,N. \tag{29}$$

By calculating the unknown dislocation density $B_{zj}(p)$ it is feasible to determine the fracture parameters, especially the stress intensity factors. So, the system of integral Eq. (27) and (29) are determined to find the dislocation density functions$B_{zj}(p)$. It should be mentioned that the stress fields behave like $1/\sqrt{r}$ in the crack tips neighborhood where r is the distance from the crack tip. The dislocation density can be expressed as

$$B_{zj}(p) = \frac{q_{zj}(p)}{\sqrt{1-p^2}}, -1 < p < 1, j = 1,2,\dots,N. \tag{30}$$

Substituting Eq. (30) into Eq. (27) and Eq. (29) and solving the resultant system of integral equations, $q_{zj}(p)$ can be calculated. So, by virtue of the crack opening displacement given in Eq. (28), the stress intensity factors could be written for the tip of i-th crack as follows

$$K_{\mathrm{III}R_i} = \frac{\sqrt{2}}{4} g G_y \lim_{r_{R_i}\to 0} \frac{w_i^-(\omega) - w_i^+(\omega)}{\sqrt{r_{R_i}}}, \quad K_{\mathrm{III}L_i} = \frac{\sqrt{2}}{4} g G_y \lim_{r_{L_i}\to 0} \frac{w_i^-(\omega) - w_i^+(\omega)}{\sqrt{r_{L_i}}}. \tag{31}$$

Subscripts R and L are the right and left tips of a crack respectively. The geometry of a crack denotes

$$r_{R_i} = [(x_i(\omega) - x_i(1))^2 + (y_i(\omega) - y_i(1))^2]^{\frac{1}{2}},$$
$$r_{L_i} = [(x_i(\omega) - x_i(-1))^2 + (y_i(\omega) - y_i(-1))^2]^{\frac{1}{2}}. \quad (32)$$

Consequently, the modes III stress intensity factors for embedded cracks are

$$K_{\mathrm{III}R_i} = -\frac{gG_y}{2}[(x'_i(1))^2 + (y'_i(1))^2]^{\frac{1}{4}} q_{zi}(1),$$
$$K_{\mathrm{III}L_i} = \frac{gG_y}{2}[(x'_i(-1))^2 + (y'_i(-1))^2]^{\frac{1}{4}} q_{zi}(-1), i = 1,2,\ldots,N. \quad (33)$$

To determine stress intensity factors, the results for$q_{zi}(\pm 1)$ should be calculated utilizing the technique developed by Erdogan et al. [28].

5 Results and discussions

The first validity of solution is examined by considering $h_1 \to 0$ in our results for single crack and two cracks located in the center line of an orthotropic strip under point load with those given by Ayatollahi et al. [29]. The dimensionless DSIFs versus the dimensionless crack velocity ($c = V/C_p$) plotted in Figure (2) and Figure (3) for one crack and two cracks respectively. It can be observed that the present results agree very well with [29].
In the second verification, we compare the effects of the dimensionless electric field on the normalized stress intensity factors. According to Figure (4), the SIFs values decrease steadily so long as the electric field increases. The electric filed is normalized by $D^* = c_{44}e_{15}D_0/\alpha_1 d_{11}\tau_0$.

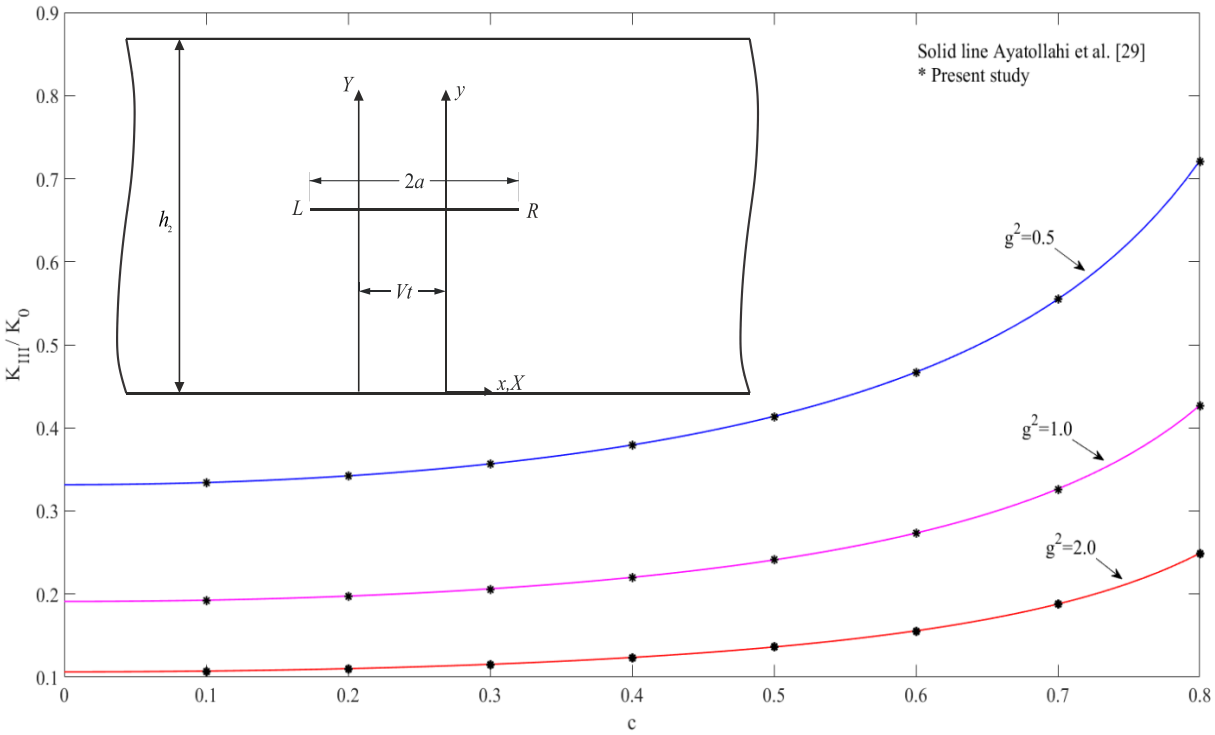

Figure 2 Comparison of normalized SIFs for a central crack in an orthotropic strip

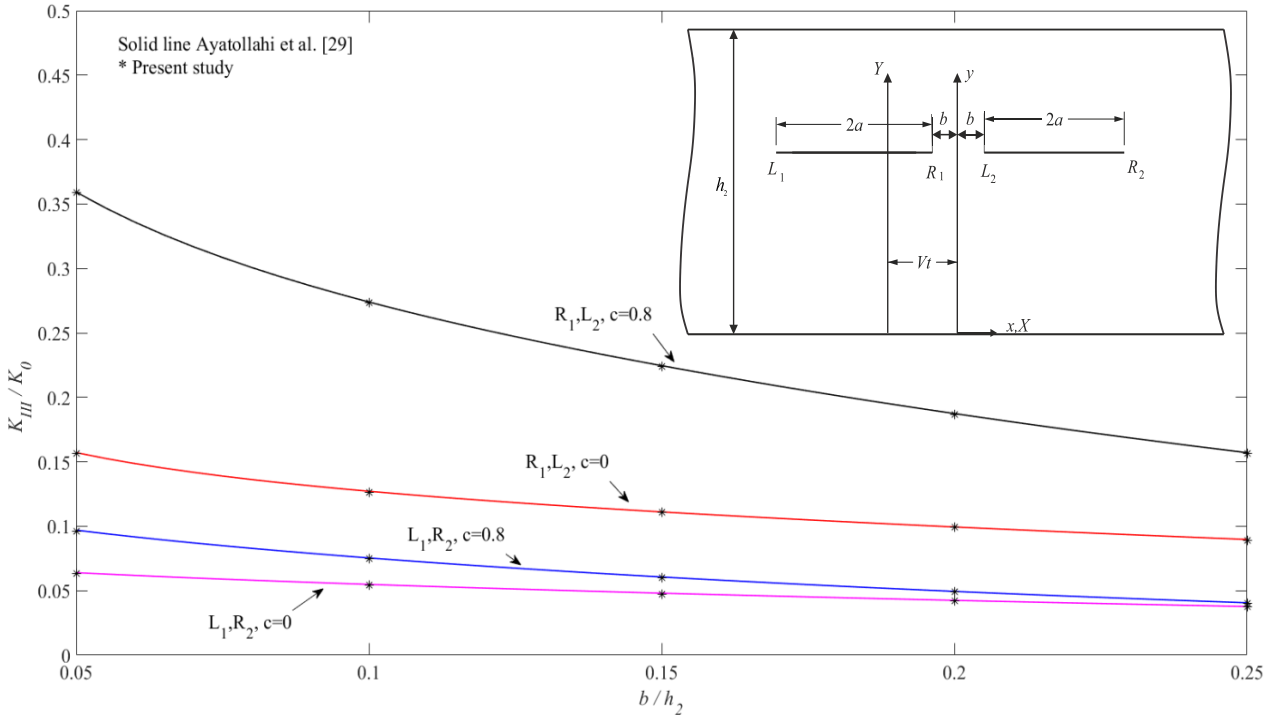

Figure 3 Comparison of normalized SIFs for two central cracks in an orthotropic strip.

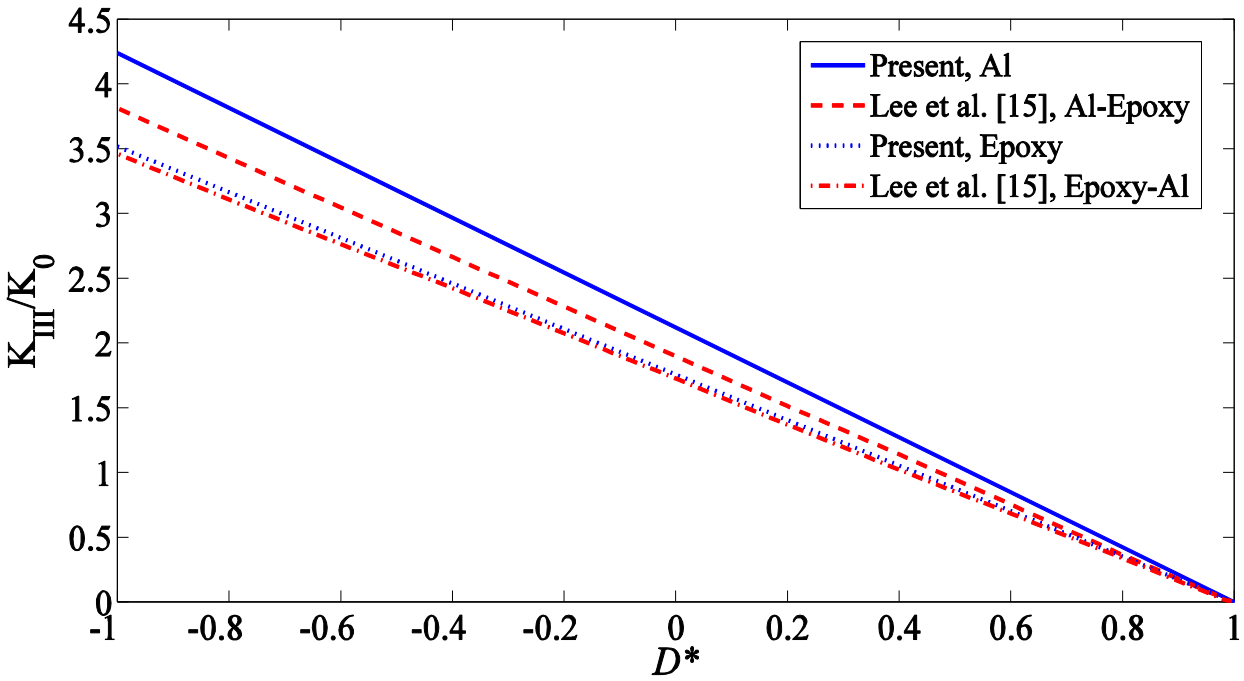

Figure 4 Comparison of normalized stress intensity factors versus dimensionless electric field (Case I, PZT-5, $d = h_2/20$, $h_1 = h_2 = 1$, $\kappa h_2 = 0$, $c = 0.5$)

This phenomenon illustrates that the crack opening is highly influenced by the electric loading which can control and minimize the crack growth. Also, the results show the same behavior with those found by Lee et al. [15]. However, it is worth mentioning that the results provided in [15] are for an interface crack between two orthotropic layers and piezoelectric coating. To compensate the difference between the present investigation and the mentioned study, the crack is located near of the piezoelectric layer.

At this section numerous examples are solved to show the effect of crack configuration, nonhomogeneity parameter and material properties on the stress intensity factors. In the numerical results, PZT-4 and PZT-5 with the material properties given in Table (1) are considered and also three different material properties for the orthotropic layer given in Table (2). The geometric parameters of layers structure will be assumed in advance such as$h_2 = 0.1m$ and $h_1 = 0.1h_2$. The dimensionless crack length is considered to be $a/h_2 = 0.5$ unless it is stated for each specific example. Besides, in the following examples, three different loadings s applied to the boundaries namely, electromechanical point load, constant shear stress which is defined by pure mechanical load τ_0, dielectric displacement D_0 and uniform shear stress τ_0 which are illustrated in section (3). The stress intensity factors are normalized by $K_0 = \tau_0\sqrt{a}$ for the uniform shear loading and by $K_0 = \tau_0/\sqrt{a}$ for point loads unless it is stated for the specific examples. Figure (5) shows a one crack in an orthotropic layer under electromechanical loading.

As can be seen, SIFs for various material properties under loading Case II and Point Load are given in Figures (6). Based on Figure (6a), by increasing the crack length, the SIFs escalates dramatically which is in contrast to the results provided in Figure (6b), where the SIFs show a downward trend after a considerable rise. It also can be seen that PZT-5 allocates slightly more SIFs values than PZT-4. Also, it is clear that isotropic material has considerably more stress intensity values than the orthotropic material.

According to Figures (7), the normalized crack velocity has a significant impact on the SIFs. Uniform loading (Case II) and point load are applied on the boundaries respectively. The SIFs are influenced drastically by the orthotropic constants in which the stress intensity factors plummets as the shear modulus ratio increase. Also it is seen that the piezoelectric materials have less effect on the stress intensity factor due to the closeness of the material properties. Furthermore, as expected, uniform distributed loading (Case II), has considerably more SIF values than the applied point load which acts at a single point.

On the other example, depicted in Figures (8), the effect of diverse loadings namely Case I, Case II and point load which determined in section (3), on the stress intensity factors are given. What is more, as seen in Figure (4) the minimum amount of SIFs were calculated when $D^* = 1$. Consequently, this amount of electric loading is applied on the boundary so that the SIFs would be minimal. As can be seen in Figure (8a), Case I has the least amount of SIFs which is approximately equal to zero. However, Case II has by far the most SIFs values and rises as crack length increases. In contrast, the applied point load escalates and then declines as long as the non-dimensional crack length increases. On the other hand, as can be seen in Figure (8b), the SIFs show an upward trend as dimensionless crack speed increases. Case II has the most amounts of SIFs as opposed to Case I which is almost zero.

Table 1 Material properties for piezoelectric coating Lee et al. [15] and Bagheri et al. [15]

Material	$c_{44}^0(Pa)$	$e_{15}^0(C/m^2)$	$d_{11}^0(C/Vm)$	$\rho_{piezo}^0(kg/m^3)$
PZT-4	2.56×10^{10}	12.7	64.6×10^{-10}	7500
PZT-5	2.11×10^{10}	12.3	81.1×10^{-10}	7750

Table 2 Material properties for orthotropic layer Lee et al. [15]

Materials	$G_x(GPa)$	$G_y(GPa)$	$\rho_{ortho}(kg/m^3)$	$g = \sqrt{G_x/G_y}$
Aluminum	26.5	26.5	2800	1
Graphite-Epoxy	5.65	3.61	1590	1.25
Epoxy	1.76	1.76	1150	1

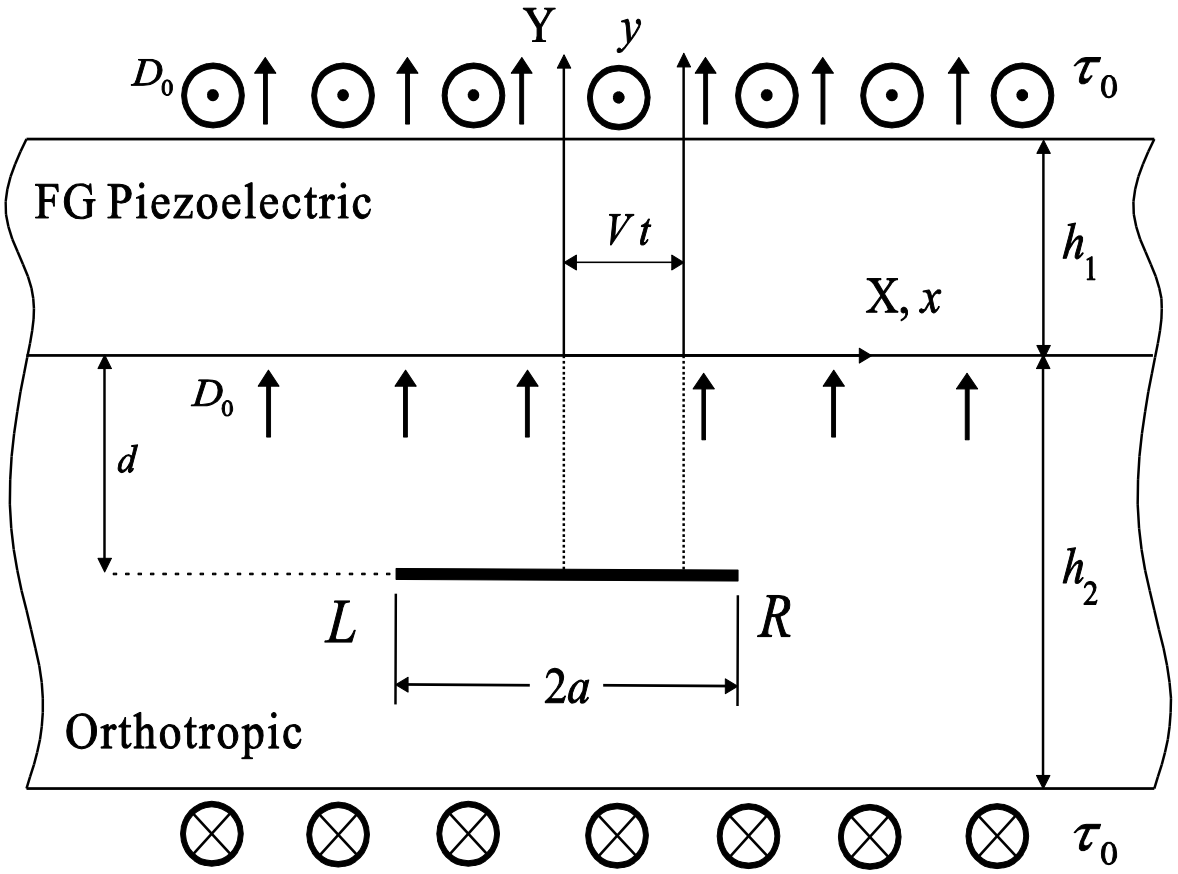

Figure 5 Geometry and schematic of a medium containing one crack under electromechanical loading

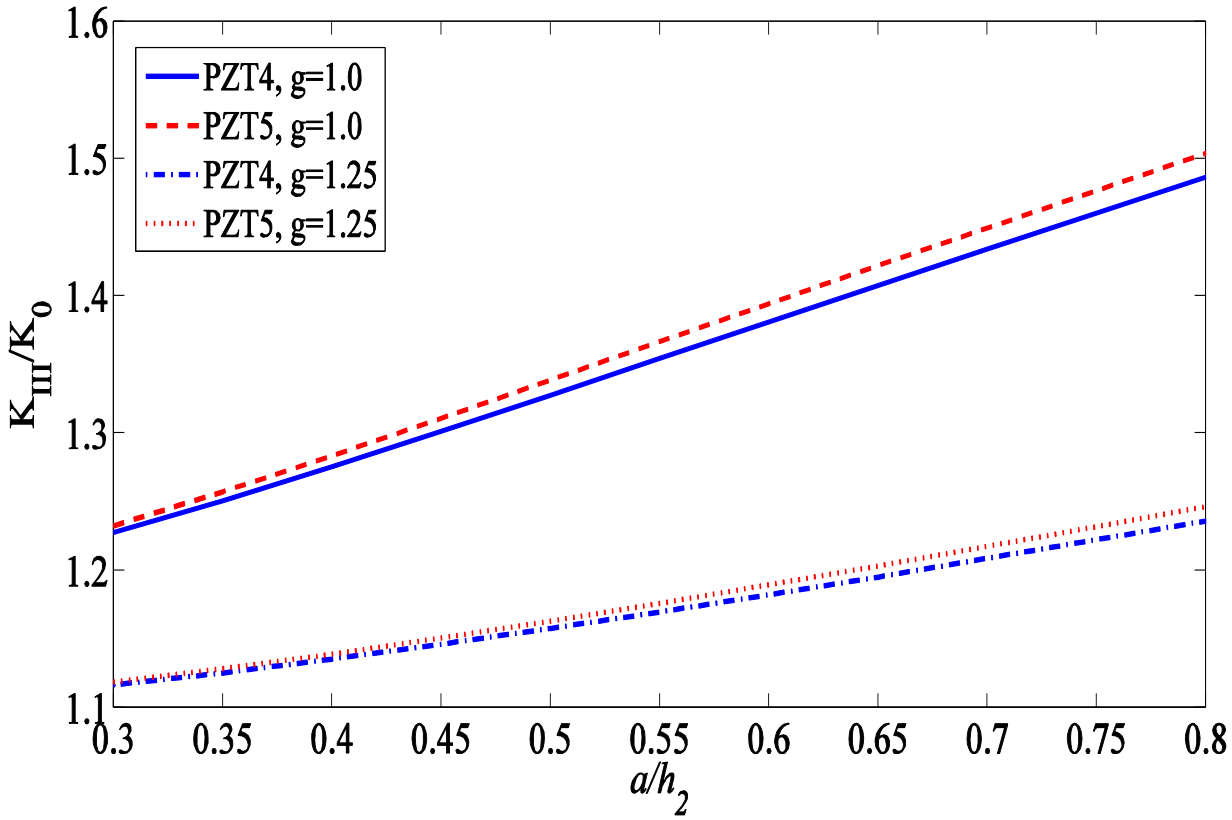

Figure 6a Normalized stress intensity factors versus crack length (Case II, $\kappa h_2 = 1$, $c = 0.5$, $d = h_2/2$)

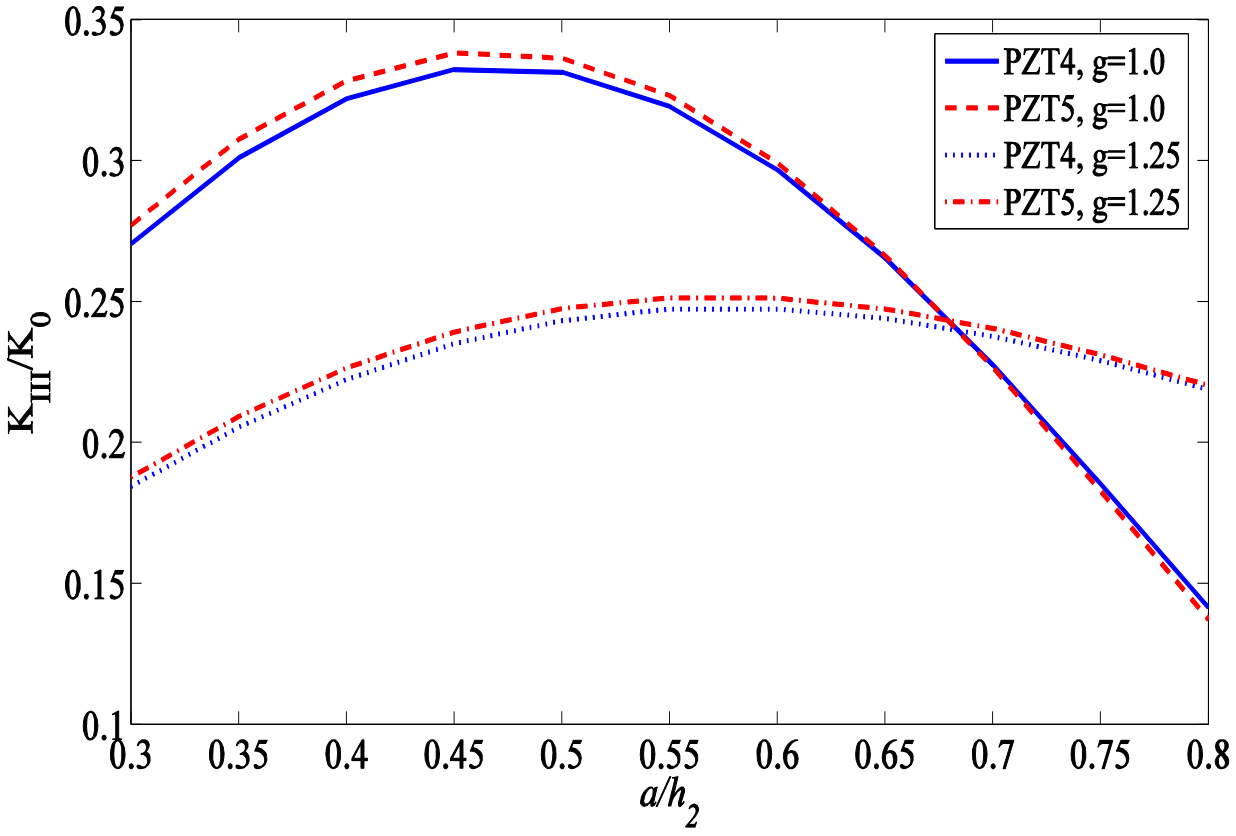

Figure 6b Normalized stress intensity factors versus crack length (Point Load, $\kappa h_2 = 1$, $c = 0.5$, $d = h_2/2$)

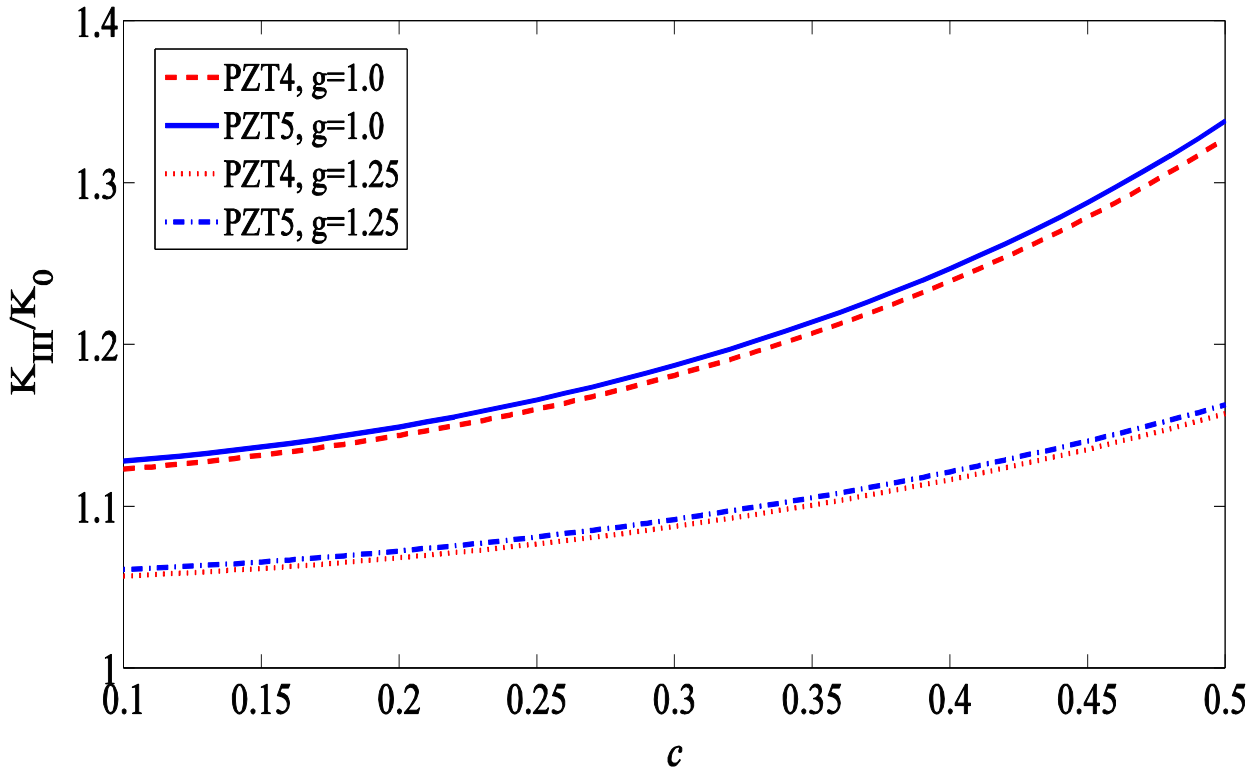

Figure 7a Normalized stress intensity factors versus crack velocity (Case II, $a/h_2 = 0.5$, $\kappa h_2 = 1$,$d = h_2/2$)

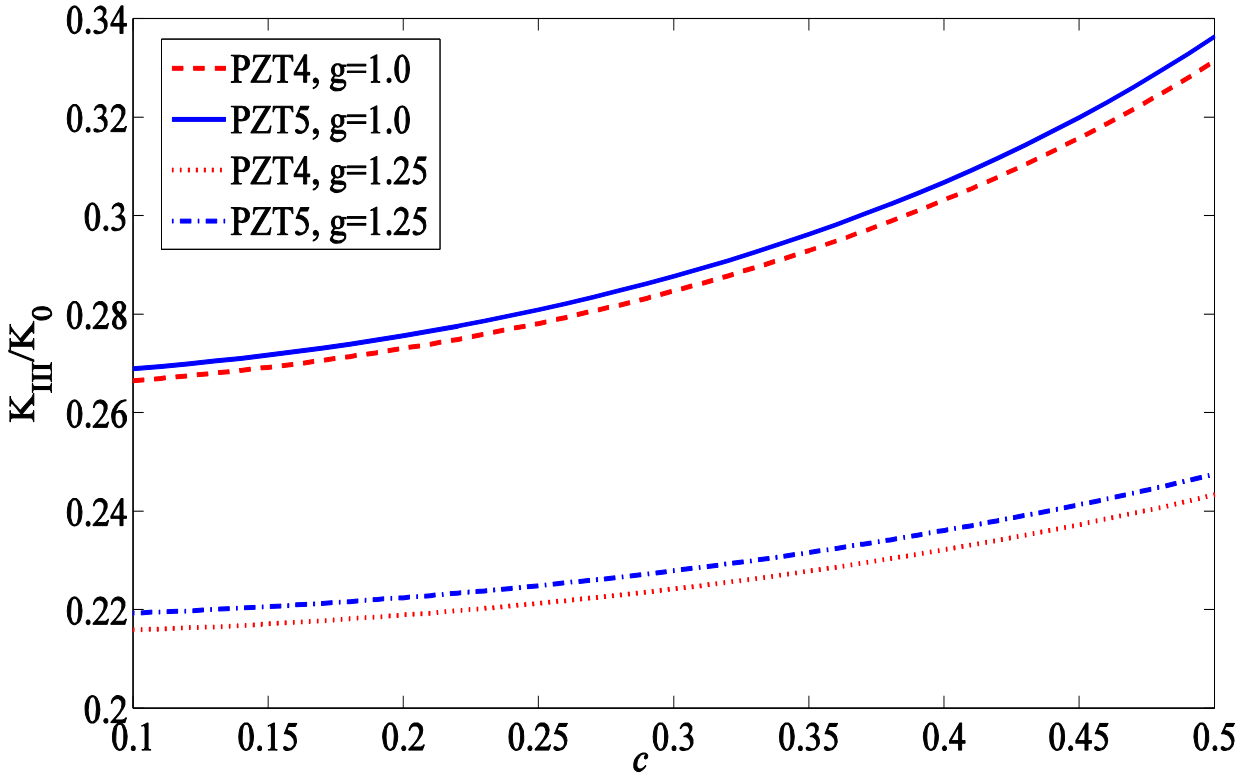

Figure 7b Normalized stress intensity factors versus crack velocity (Point Load, $a/h_2 = 0.5$, $\kappa h_2 = 1$,$d = h_2/2$)

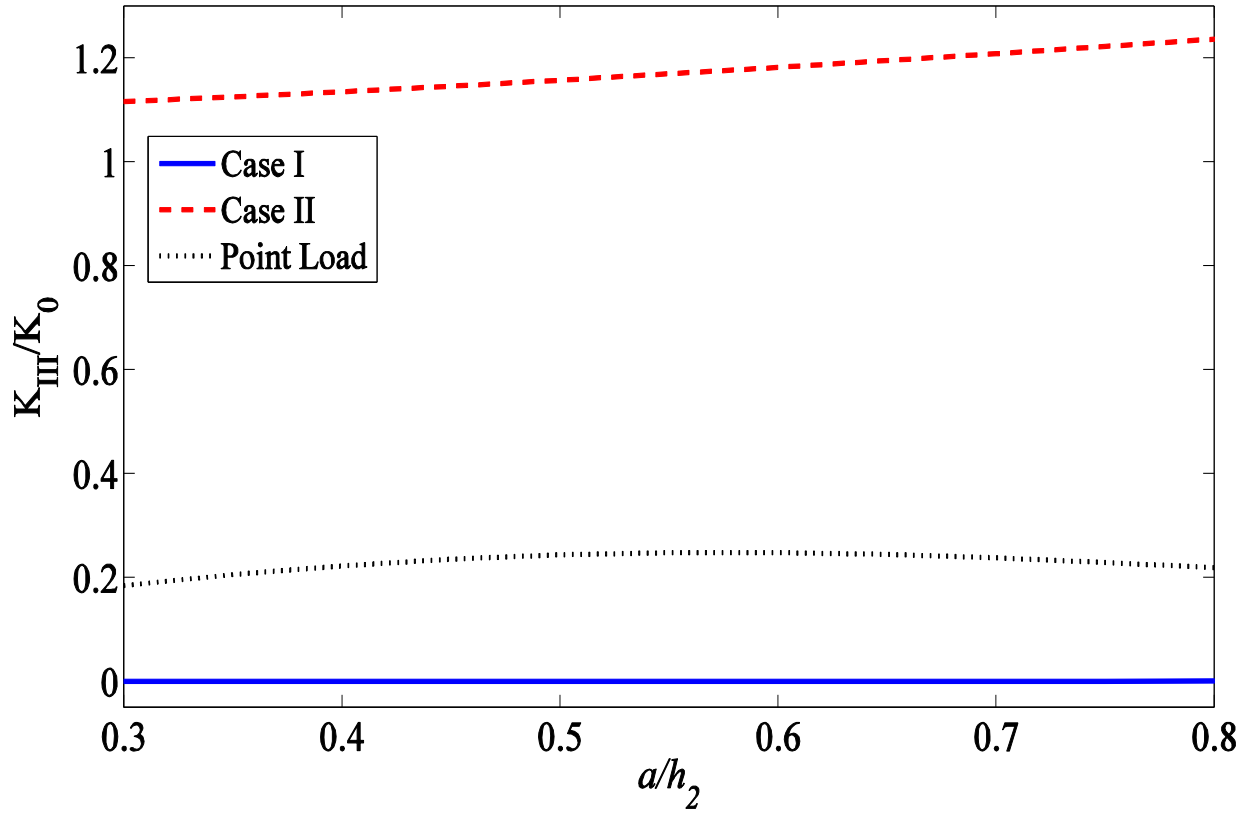

Figure 8a Effect of various loadings on normalized stress intensity factors versus crack length ($c = 0.5$,$g = 1.25$, $\kappa h_2 = 1$, PZT-4, $d = h_2/2$)

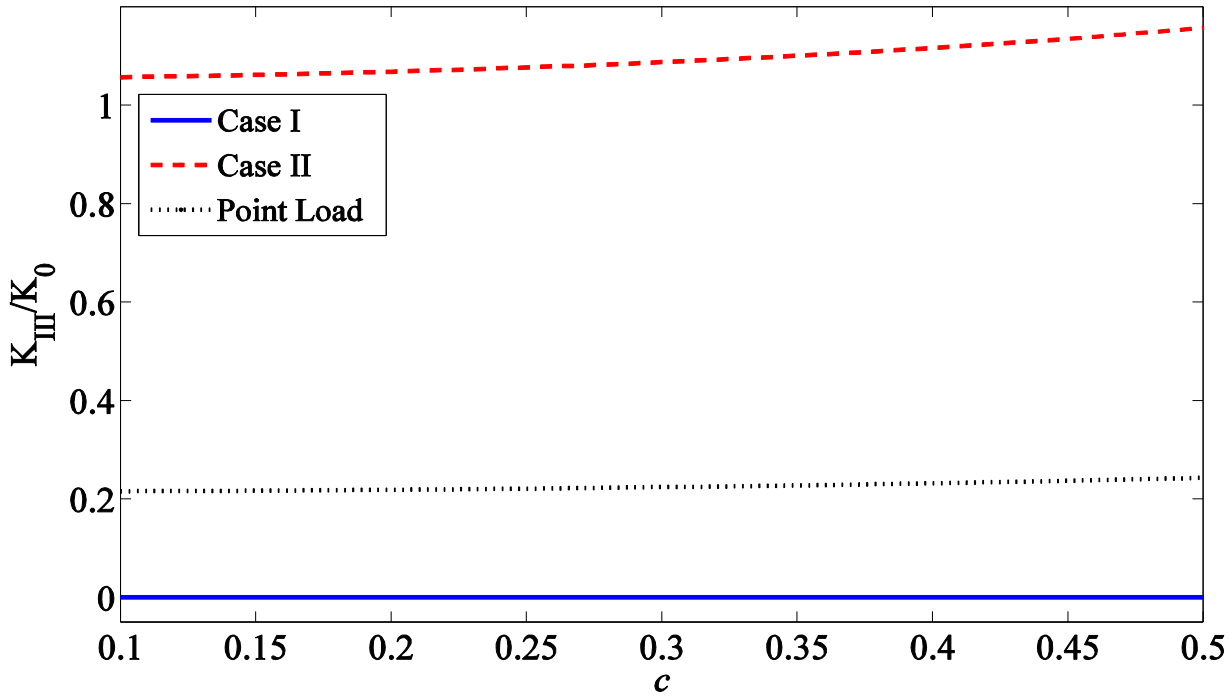

Figure 8b Effect of various loadings on normalized stress intensity factors versus crack speed ($a/h_2 = 0.5$,$g = 1.25$, $\kappa h_2 = 1$, PZT-4, $d = h_2/2$)

Table 3 Comparison of loading types on the stress intensity factors for PZT-4 ,$g = 1.25$ and $c = 0.5$

Types of Loadings		$\frac{a}{h_2} = 0.3$	$\frac{a}{h_2} = 0.5$	$\frac{a}{h_2} = 0.9$
Case I	$\kappa h_2 = 0$	0.0053	0.0058	0.0061
	$\kappa h_2 = 1$	0.0053	0.0057	0.0060
Case II	$\kappa h_2 = 0$	1.1171	1.1594	1.2688
	$\kappa h_2 = 1$	1.1163	1.1575	1.2644
Point Load	$\kappa h_2 = 0$	0.1857	0.2450	0.1970
	$\kappa h_2 = 1$	0.1843	0.2433	0.1967

In another example, different type of loadings are applied and compared for various crack length and non-homogeneity parameter values (Table (3)). In this example the applied electrical loading is also considered to be $D^* = 1$. As can be seen, the SIFs for Case I have approximately zero values which indicate that by applying this amount of dielectric loading along with the pure mechanical loading on the boundaries, the crack opening may be minimal. Moreover, the point load allocates the second least amount of SIFs which was fully explained in the previous examples as well. On the contrary, Case II has by far the most SIFs values. Case I and II SIFs show an upward trend as crack length increases, and, non-homogeneity parameter decreases. Figure (9) demonstrations two parallel cracks in an orthotropic layer under electromechanical loading.

In the next example, as shown in Figure (10) and Figure (11), the effect of crack length and velocity of two parallel cracks with the distance $x_c/h_2 = 0.5$ on the stress intensity factors under point load and Case II are investigated. As it was expected the highest stress intensity factor occurs where the distance between the interacting crack tips L_1 and R_2 is minimal. For larger values of a/h_2, crack tip L_1 passes crack tip R_2 reducing stress intensity factor at L_1 and R_2 while enhancing it at R_1 and L_2. Moreover, the SIFs rises gradually as dimensionless crack speed increases. What is more, left crack tips have slightly less SIFs values than the right crack tips in both examples.

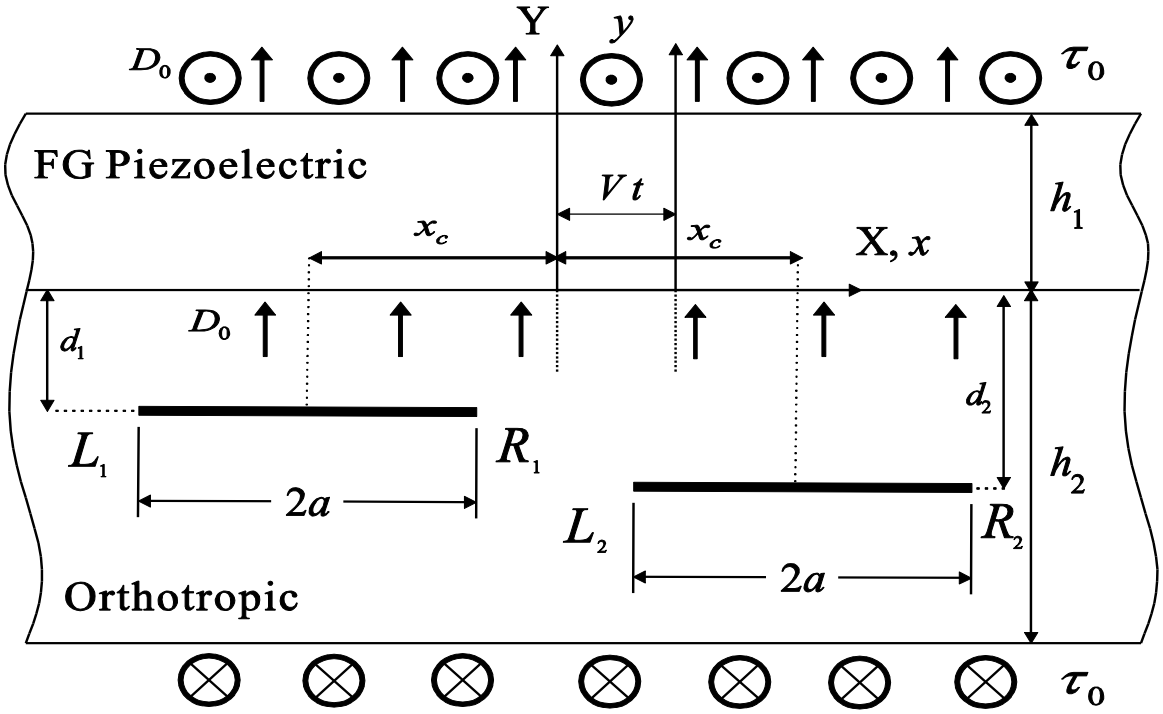

Figure 9 Geometry and schematic of a medium containing two parallel cracks under electromechanical loading

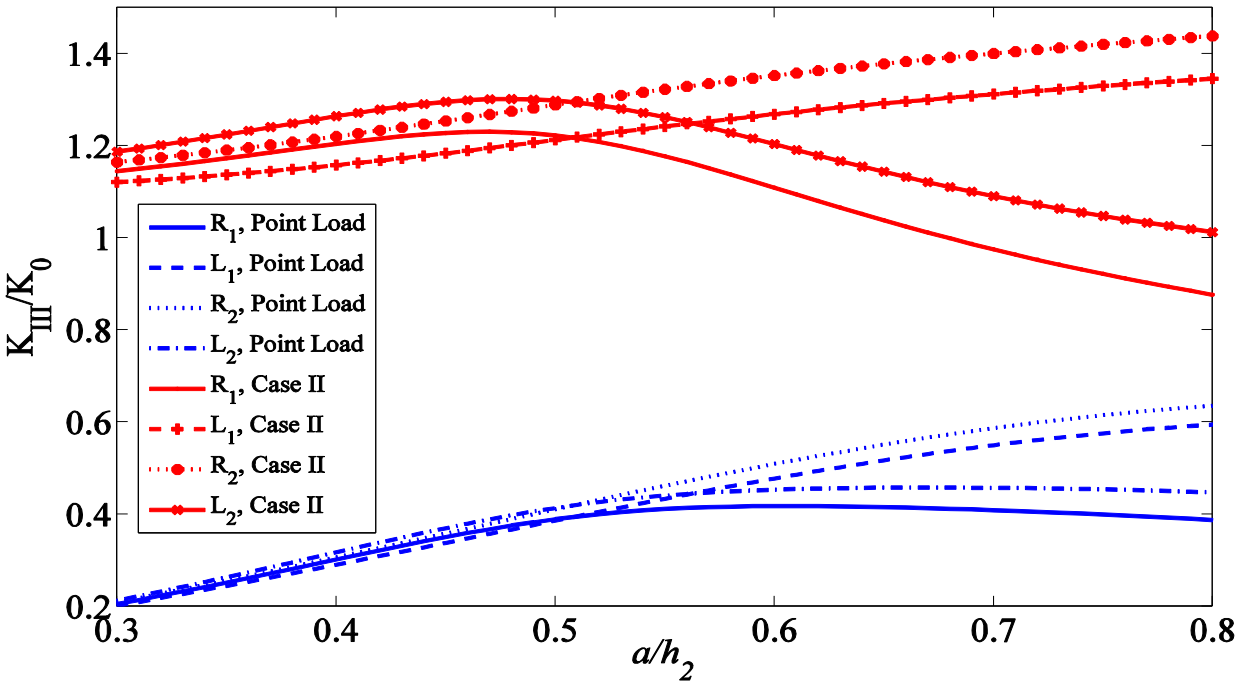

Figure 10 Normalized stress intensity factors for two parallel cracks versus cracks length ($PZT\text{-}4, \kappa h_2 = 1, c = 0.5, g = 1.25, x_c = 0.5h_2, d_1 = h_2/4, d_2 = h_2/2$)

In the last example, two identical parallel cracks are investigated. Cracks are located exactly above each other (see Figure (12)). According to Figures (13) and Figure (14), crack tips R_1 ,L_1 and R_2, L_2 have the same amount of SIFs due to the symmetry of the problem. It can be seen that the Case II allocates far more SIFs values than point load. Besides, it is evident that as dimensionless crack length and dimensionless crack speed increases, SIF values rises steadily. In this arrangement crack, it is seen that the interaction effect is weaker and produces a shielding effect, thus SIFs of two cracks are less than those of SIFs of one crack with the same conditions.

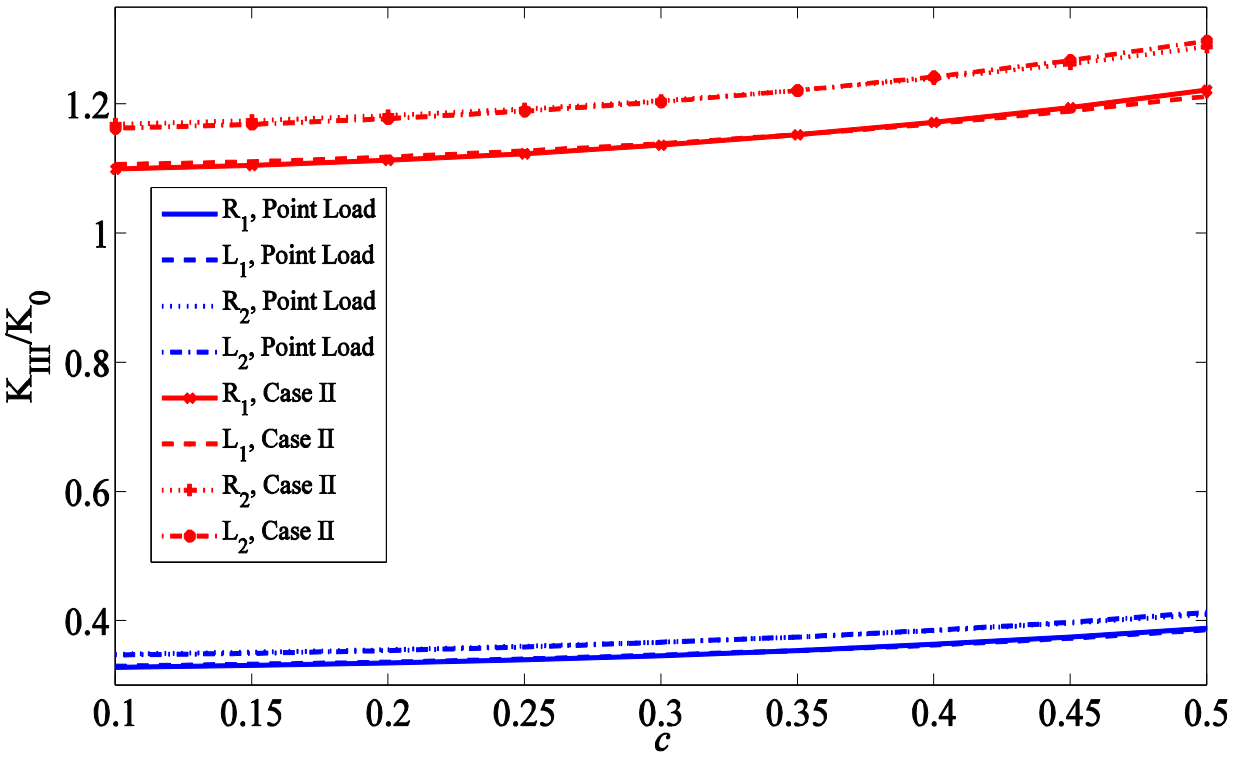

Figure 11 Normalized stress intensity factors for two parallel cracks versus cracks velocity for material (PZT-4,$\kappa h_2 = 1, a/h_2 = 0.5$, $g = 1.25$, $x_c = 0.5h_2$, $d_1 = h_2/4$, $d_2 = h_2/2$)

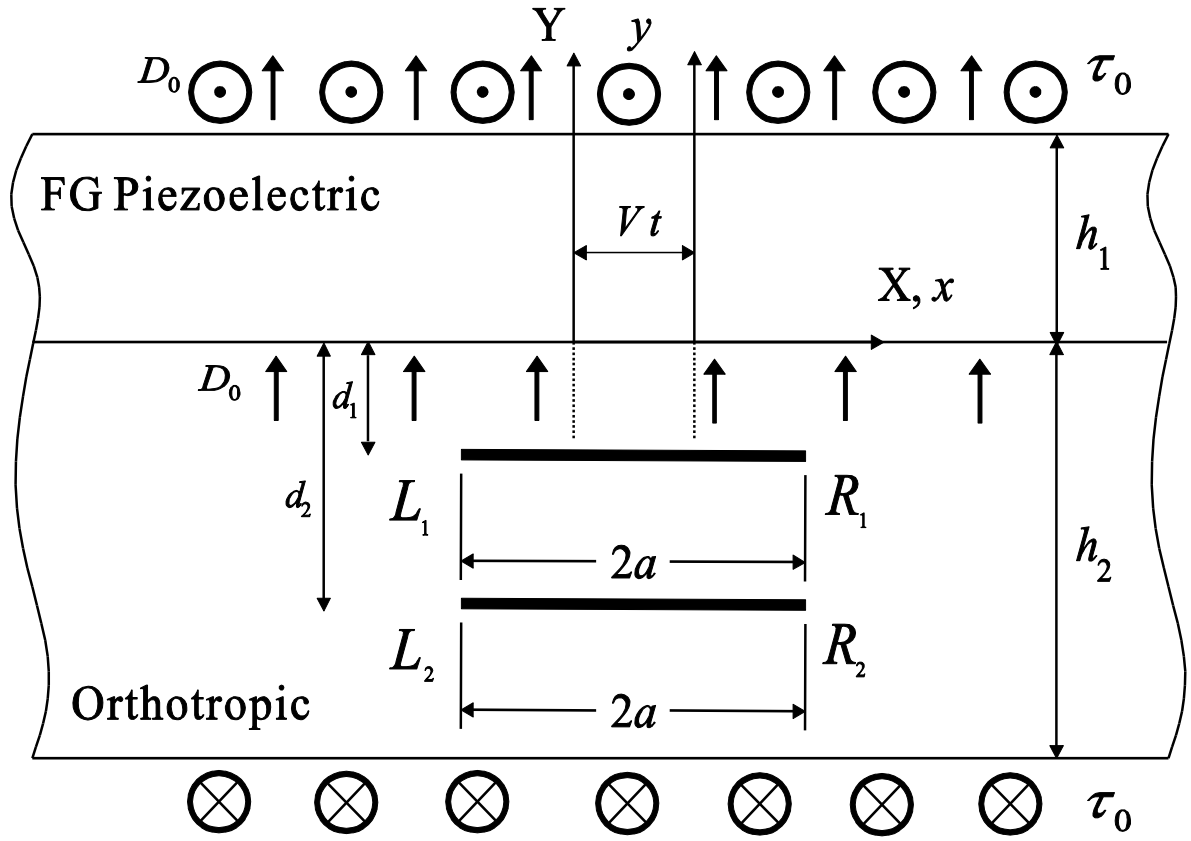

Figure 12 Geometry and schematic of a medium containing two identical parallel cracks above each other under electromechanical loading

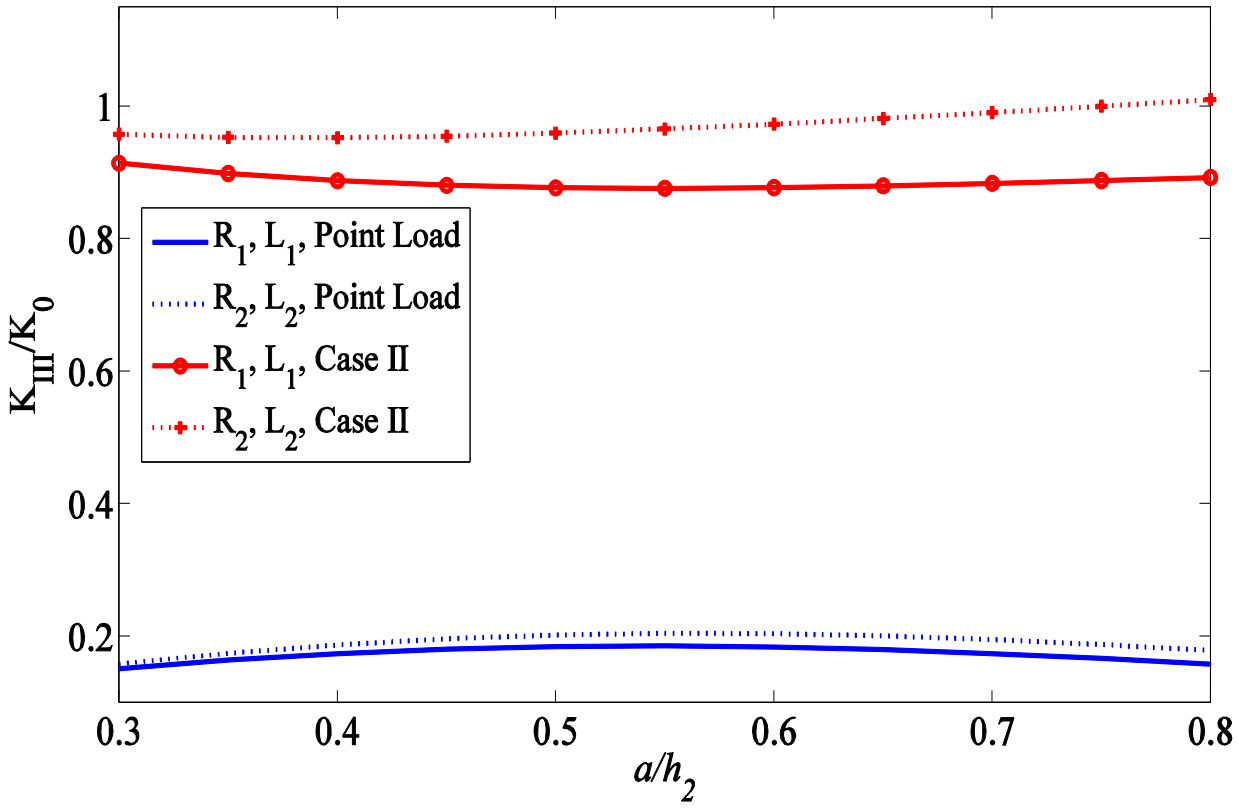

Figure 13 Normalized stress intensity factors for two identical parallel cracks versus cracks length (PZT-4,$\kappa h_2 = 1, c = 0.5, = 1.25\ , d_1 = h_2/4, d_2 = h_2/2$)

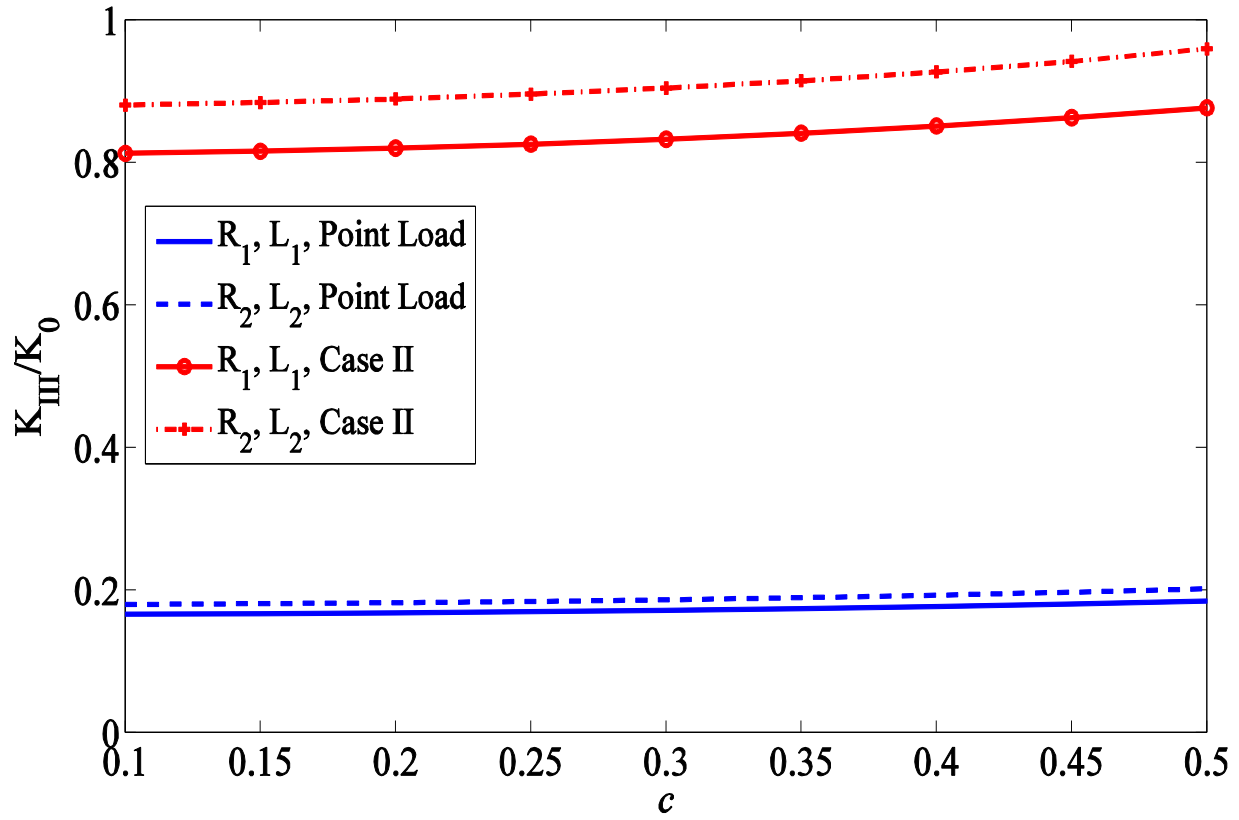

Figure 14 Normalized stress intensity factors for two identical parallel cracks versus cracks length (PZT-4,$\kappa h_2 = 1, a/h_2 = 0.5, = 1.25\ , d_1 = h_2/4, d_2 = h_2/2$)

6 Conclusions

The presented investigation deals with the fracture analysis of multiple moving cracks in an orthotropic layer bonded to a functionally graded piezoelectric coating under different type of loading. At first, with the help of the distributed dislocation technique the stress fields in an orthotropic layer weakened by a screw-type dislocation are obtained. By using the dislocation solution the integral equations are derived with a known Cauchy type singularity. Then, several examples are solved to show the effects of material properties, nonhomogeneity parameter, crack length and crack speed on the stress intensity factors. It was seen that

1. The stress intensity factors are highly influenced by the dielectric loading.
2. The dielectric loading can considerably reduce the stress intensity factors.
3. Case II uniform loading allocates by far the most amounts of stress intensity factors.
4. While Case I is applied on the boundaries, the stress intensity factors are approximately zero. Point load has considerably less amount of stress intensity factors as opposed to Case II.
5. As dimensionless crack length and crack speed increases, the stress intensity factors increase gradually.
6. By increasing the ratio of the shear modulus and non-homogeneity parameter, the stress intensity factors decrease.

References

[1] E. Carrera, S. Brischetto, and P. Nali, "*Plates and Shells for Smart Structures: Classical and Advanced Theories for Modeling and Analysis*," John Wiley & Sons, Ltd., 1st edition, Vo. 36, 2011, https://onlinelibrary.wiley.com/doi/book/10.1002/9781119950004.

[2] K. Ichikawa, "*Functionally Graded Materials in the 21st Century: A Workshop on Trends and Forecasts*," 1st edition, Springer Science & Business Media, Springer US, 2001, https://link.springer.com/book/10.1007/978-1-4615-4373-2.

[3] Y. Miyamoto, W. A. Kaysser, B. H. Rabin, A. Kawasaki, and R. G. Ford, "*Functionally Graded Materials: Design, Processing and Applications*," Springer Science & Business Media, LLC, Vol. 5, 2013, doi: 10.1007/978-1-4615-5301-4, https://link.springer.com/book/10.1007/978-1-4615-5301-4.

[4] L. Ma, L. Z. Wu, Z. G. Zhou, and L. C Guo, "Scattering of the Harmonic Anti-plane Shear Waves by a Crack in Functionally Graded Piezoelectric Materials," *Composite Structures*, Vol. 69, No. 4, pp. 436-441, 2005, https://doi.org/10.1016/j.compstruct.2004.08.001.

[5] X. F. Li, T. Y. Fan, and X. F. Wu, "A Moving Mode-III Crack at the Interface between Two Dissimilar Piezoelectric Materials," *International Journal of Engineering Science*, Vol. 38, No. 11, pp. 1219-1234, 2000, https://doi.org/10.1016/S0020-7225(99)00072-5.

[6] J. W. Shin, and Y. S. Lee, "A Moving Interface Crack between Two Dissimilar Functionally Graded Piezoelectric Layers under Electromechanical Loading," *International Journal of Solids and Structures*, Vol. 47, No. 20, pp. 2706-2713, 2010, https://doi.org/10.1016/j.ijsolstr.2010.05.027.

[7] Y. Lapusta, A. Komarov, F. L. Jied, R. M. Pitti and, V. Loboda," Limited Permeable Crack Moving Along the Interface of a Piezoelectric Bi-Material," *European Journal of*

Mechanics-A/Solids, Vol. 30, No. 5, pp. 639-649, 2011, https://doi.org/10.1016/j.euromechsol.2011.04.005.

[8] M. Ayatollahi, and M. M. Monfared, "Anti-plane Transient Analysis of Planes with Multiple Cracks," *Mechanics of Materials*, Vol. 50, pp. 36-46, 2012, https://doi.org/10.1016/j.mechmat.2012.03.002.

[9] M. M. Monfared, and M. Ayatollahi, "Dynamic Stress Intensity Factors of Multiple Cracks in a Functionally Graded Orthotropic Half-plane," *Theoretical and Applied Fracture Mechanics*, Vol. 56, No. 1, pp. 49-57, 2011, https://doi.org/10.1016/j.tafmec.2011.09.008.

[10] A. Hejazi, M. Ayatollahi, R. Bagheri, and M.M. Monfared, "Dislocation Technique to Obtain the Dynamic Stress Intensity Factors for Multiple Cracks in a Half-plane under Impact Load," *Archive of Applied Mechanics*, Vol. 84, No. 1, pp. 95-107, 2014, https://doi.org/10.1007/s00419-013-0785-y.

[11] N. T. Nguyen, T.Q. Bui, and T.T. Truong, "Transient Dynamic Fracture Analysis by an Extended Meshfree Method with Different Crack-tip Enrichments," *Meccanica*, Vol. 52, No. 10, pp. 2363–2390, 2017, https://doi.org/10.1007/s11012-016-0589-6.

[12] J. Rokne, B. M. Singh, and R. S. Dhaliwal, "Moving Anti-plane Shear Crack in a Piezoelectric Layer Bonded to Dissimilar Elastic Infinite Spaces," *European Journal of Mechanics - A/Solids*, Vol. 31, No. 1, pp. 47-53, 2012, https://doi.org/10.1016/j.euromechsol.2011.07.002.

[13] J., Podgórski," The Criterion For Determining the Direction of Crack Propagation in a Random Pattern Composites," *Meccanica*, Vol. 52, No. 8, pp. 1923-1934, 2017, https://doi.org/10.1007/s11012-016-0523-y.

[14] R. Bagheri, M. Ayatollahi, and S. M. Mousavi, "Analytical Solution of Multiple Moving Cracks in Functionally Graded Piezoelectric Strip," *Applied Mathematics and Mechanics*, Vol. 36, No. 6, pp. 777-792, 2015, https://doi.org/10.1007/s10483-015-1942-6.

[15] J. S. Lee, S. M. Kwon, K. Y. Lee, and J. H. Kwon, "Anti-plane Interfacial Yoffe-Crack between a Piezoelectric and Two Orthotropic Layers," *European Journal of Mechanics - A/Solids*, Vol. 21, No. 3, pp. 483-492, 2002, https://doi.org/10.1016/S0997-7538(02)01212-3.

[16] M. M. Monfared", Mode III SIFs for Interface Cracks in an FGM Coating-Substrate System," *Structural Engineering and Mechanics*, Vol. 64, No. 1, pp. 71-79, 2017, https://doi.org/10.12989/sem.2017.64.1.071.

[17] M. Hassani, M. M. Monfared, and A. Salarvand, "Multiple Unequal Cracks between an FGM Orthotropic Layer and an Orthotropic Substrate under Mixed Mode Concentrated Loads," *Structural Engineering and Mechanics*, Vol. 86, No. 4, pp. 535-546, 2023, https://doi.org/10.12989/sem.2023.86.4.535.

[18] H. Haghiri, A. R. Fotuhi, and A.R. Shafiei, "Elastodynamic Analysis of Mode III Multiple Cracks in a Functionally Graded Orthotropic Half-plane," *Theoretical and Applied Fracture Mechanics*, Vol. 80, Part B, pp. 155-169, 2015, https://doi.org/10.1016/j.tafmec.2015.09.006.

[19] J. W. Shin, and Y. S. Lee, "Anti-plane Moving Crack in a Functionally Graded Piezoelectric Layer between Two Dissimilar Piezoelectric Strips," *Journal of Mechanical Science and Technology*, Vol. 26, No. 4, pp. 1017-1025, 2012, https://doi.org/10.1007/s12206-012-0233-x.

[20] K. Hu, and Z. Chen, "An Interface Crack Moving between Magnetoelectroelastic and Functionally Graded Elastic Layers," *Applied Mathematical Modelling*, Vol. 38, No. 3, pp. 910-925, 2014, https://doi.org/10.1016/j.apm.2013.07.022.

[21] B. Jin, and Z. Zhong, "A Moving Mode-III Crack in Functionally Graded Piezoelectric Material: Permeable Problem," *Mechanics Research Communications*, Vol. 29, No. 4, pp. 217-224, 2002, https://doi.org/10.1016/S0093-6413(02)00259-8.

[22] S. K. Alavi, M. R. Ayatollahi, J. Jamali, and M. Petru, "On the Applicability of Digital Image Correlation Method in Extracting the Higher Order Terms in Stress Field around Blunt Notches," *Theoretical and Applied Fracture Mechanics*, Vol. 121, pp. 103436, 2022, https://doi.org/10.1016/j.tafmec.2022.103436 .

[23] S. K. Alavi, M. R. Ayatollahi, M. Daneshfar, and B. Bahrami, "Experimental Stress Determination of Blunt Notches under Combinations of Modes I and II Loading," *Engineering Structures*, Vol. 278, pp. 115517, 2023, https://doi.org/10.1016/j.engstruct.2022.115517.

[24] B. Bahrami, M. R. Ayatollahi, S. K. Alavi, and L.F.M. da Silva, "On the Prediction of the Stress Field in Adhesive Joints using a Combined Analytical-Numerical Method," *International Journal of Adhesion and Adhesives*, Vol. 116, pp. 103151, 2022, https://doi.org/10.1016/j.ijadhadh.2022.103151.

[25] S. K. Alavi, M. R. Ayatollahi, B. Bahrami, and M. Nejati, "An Analytical Stress Field for Bi-Material V-Notches with end Hole: New Solution and Effects of Higher Order Terms," *Mathematics and Mechanics of Solids*, Vol. 28, No. 2, pp. 464–478, 2022, https://doi.org/10.1177/10812865221084311.

[26] J. L. Bleustein, "A New Surface Wave in Piezoelectric Materials," *Applied Physics Letters*, Vol. 13, pp. 412-413, 1968, 10.1063/1.1652495.

[27] D. A. Hills, K. P. A., Dai D. N., and A. M. Korsunsky, "Solution of Crack Problems: The Distributed Dislocation Technique," *Kluwer Academic Publishers*, 1996, https://link.springer.com/book/10.1007/978-94-015-8648-1.

[28] F. Erdogan, G. D. Gupta, and T.S. Cook, "Numerical Solution of Integral Equations," In: Sih GC, Editor. Methods of Analysis and Solution of Crack Problems. *Leyden, Holland: Noordhoof*; 1973, https://link.springer.com/chapter/10.1007/978-94-017-2260-5_7.

[29] M. Ayatollahi, R. T. Faal, and O. Tarkian, "Anti-plane Analysis of an Orthotropic Strip Weakened by Several Moving Cracks," *Applied Mathematical Modellsing*, Vol. 36, pp. 596-604, 2011, https://doi.org/10.1016/j.apm.2011.07.030.

Appendix A

The functions Q_{ij} include χ, α_1 given in Eq. (20a) and (20b) are

$$\begin{aligned} &Q_{11} = \sinh[s\gamma(h_2+\eta)],\ Q_{12} = -s\mu^2\alpha_1 \sinh(s\gamma y)\sinh(h_1\chi) \\ &Q_{13} = [\chi\cosh(h_1\chi) - \kappa\sinh(h_1\chi)]G_y\gamma\cosh(s\gamma y). \end{aligned} \tag{A-1}$$

$$\begin{aligned} &Q_{21} = \sinh[s\gamma(h_2+\eta)],\ Q_{22} = G_y\gamma\ \chi\cosh(h_1\chi)\sinh(s\gamma y), \\ &Q_{23} = [G_y\ \gamma\ \kappa\sinh(s\gamma y) - s\alpha_1\mu^2\cosh(s\gamma y)]\sinh(h_1\chi). \end{aligned} \tag{A-2}$$

$$\begin{aligned} &Q_{31} = \cosh[s\gamma(h_2+y)],\ Q_{32} = G_y\gamma\ \chi\cosh(h_1\chi)\sinh(s\gamma\eta) \\ &Q_{33} = [G_y\ \gamma\ \kappa\sinh(s\gamma\eta) + s\alpha_1\mu^2\cosh(s\gamma\eta)]\sinh(h_1\chi). \end{aligned} \tag{A-3}$$

$$\begin{aligned} &Q_{41} = \sinh[s\gamma(h_2+y)],\ Q_{42} = G_y\gamma\ \chi\cosh(h_1\chi)\sinh(s\gamma\eta) \\ &Q_{43} = [G_y\ \gamma\ \kappa\sinh(s\gamma\eta) + s\alpha_1\mu^2\cosh(s\gamma\eta)]\sinh(h_1\chi). \end{aligned} \tag{A-4}$$

$$\chi = \sqrt{s^2\mu^2+\kappa^2},\ \ \alpha_1 = (c_{44}+e_{15}\alpha). \tag{A-5}$$

Appendix B

The functions F and L_{ij} given in Eq. (23)

$$\begin{aligned} &L_{11} = 4s\gamma G_y\chi\ d_{11}\tau_0\cosh[s(h_2+y)\gamma], \\ &L_{12} = e^{h_1(\kappa-\chi)+sy\gamma}d_{11}\tau_0[\alpha_1(\chi-\kappa)+s\gamma G_y](\chi+\kappa), \\ &L_{13} = e^{h_1(\kappa+\chi)-sy\gamma}sd_{11}\tau_0[s\alpha_1\mu^2+\gamma G_y(\chi-\kappa)], \\ &L_{14} = e^{h_1(\kappa+\chi)+sy\gamma}d_{11}\tau_0[\alpha_1(\chi+\kappa)-s\gamma G_y](\chi-\kappa), \\ &L_{15} = e^{h_1(\kappa-\chi)-sy\gamma}sd_{11}\tau_0[s\alpha_1\mu^2-\gamma G_y(\chi+\kappa)], \\ &L_{16} = 4D_0\ e_{15}s\gamma G_y\ [-\chi + e^{h_1\kappa}(\chi\cosh(h_1\chi) - \kappa\sinh(h_1\chi))]\cosh[s(h_2+y)\gamma]. \end{aligned} \tag{B-1}$$

$$\begin{aligned} &L_{21} = \ e^{h_1(\kappa+\chi)}d_{11}\tau_0[s(s\alpha_1\mu^2-\gamma G_y(\kappa-\chi)) - e^{2sy\gamma}(\kappa-\chi)(-s\gamma G_y+\alpha_1(\kappa+\chi))], \\ &L_{22} = -4s\gamma\chi G_y\sinh[s(h_2+y)\gamma](D_0e_{15}+d_{11}\tau_0), \\ &L_{23} = 2e^{(\kappa-\chi)h_1}sd_{11}\tau_0[s\alpha_1\mu^2\cosh(sy\gamma)+\gamma G_y(\kappa+\chi)\sinh(sy\gamma)], \\ &L_{24} = -4e^{\kappa h_1}D_0e_{15}s\gamma G_y\sinh[s(h_2+y)\gamma][\chi\cosh(h_1\chi)-\kappa\sinh(h_1\chi)]. \end{aligned} \tag{B-2}$$

$$\begin{aligned} F = 2\ d_{11}\pi[&s\ \alpha_1\mu^2\cosh(h_2\ s\ \gamma)\sinh(h_1\chi) \\ &+\gamma\ G_y\sinh(h_2\ s\ \gamma)\{\chi\cosh(h_1\ \chi) - \kappa\sinh(h_1\ \chi)\}]. \end{aligned} \tag{B-3}$$